Journal Pre-proof

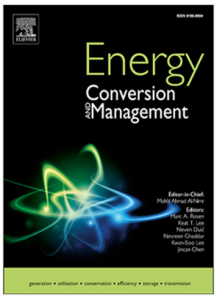

Optimization of the propulsion plant of a Liquefied Natural Gas transport ship

Andrés Meana-Fernández, Bernardo Peris-Pérez, Antonio J. Gutiérrez-Trashorras, Santiago Rodríguez-Artime, Juan Carlos Ríos-Fernández, Juan Manuel González-Caballín

PII: S0196-8904(20)30933-X
DOI: https://doi.org/10.1016/j.enconman.2020.113398
Reference: ECM 113398

To appear in: *Energy Conversion and Management*

Received date : 16 June 2020
Revised date : 18 August 2020
Accepted date : 29 August 2020

Please cite this article as: A. Meana-Fernández, B. Peris-Pérez, A.J. Gutiérrez-Trashorras et al., Optimization of the propulsion plant of a Liquefied Natural Gas transport ship. *Energy Conversion and Management* (2020), doi: https://doi.org/10.1016/j.enconman.2020.113398.

Optimization of the propulsion plant of a Liquefied Natural Gas transport ship

Andrés Meana-Fernández[a,*], Bernardo Peris-Pérez[a,b], Antonio J. Gutiérrez-Trashorras[a], Santiago Rodríguez-Artime[a], Juan Carlos Ríos-Fernández[a], Juan Manuel González-Caballín[a]

[a] *Thermal Engines and Motors Area, Department of Energy, University of Oviedo C/Wifredo Ricart s/n Gijón Asturias 33204 Spain*
[b] *Escuela Técnica Superior de Ingeniería, Grupo de Termotecnia, Universidad de Sevilla, Camino de los Descubrimientos s/n Sevilla 41092 Spain*

Abstract

Stricter emission regulations and variability of fuel prices pose the focus on the optimization of steam turbine based propulsion plants of Liquefied Natural Gas (LNG) ships. The efficiency of such a propulsion plant has been improved in this work by studying the introduction of reheating and preheating stages in the onboard regenerative Rankine cycle. A thermodynamic model of the propulsion plant has been developed from the facility diagrams, being validated afterwards with available experimental data from actual ship operation. The predictions of different scenarios obtained by the model when introducing modifications in the power propulsion cycle showed promising results. It was found that a combination of preheating and reheating stages was found to increase the cycle efficiency up to 33.71%, reducing fuel consumption in around 20 t/day and CO_2 emissions in more than 20,000 t per year. An exergy analysis of the impact of cycle modifications and an economic assessment of the proposed investment plan were performed. It was found that the boiler was the main contributor to exergy destruction, fact that justifies the cycle modifications performed. The economic analysis of the investment plan of implementing the selected alternative provided benefits even in a conservative scenario, with an Internal Rate of Return higher than 12% and a Pay-Back Period less than 9 years for all the studied scenarios. In summary, a practical industrial application of thermodynamic and exergy analysis to the propulsion plant of a LNG ship has been shown, allowing an efficiency, economic and environmental improvement.

Keywords: ocean transportation, LNG ship, propulsion efficiency, thermodynamic optimization, steam Rankine cycle

Nomenclature

*Corresponding author: andresmf@uniovi.es

$\bar{e}_i^{CH}$	specific chemical exergy of i-th component of the mixture $[kW/kg]$
$\bar{R}$	Universal gas constant = 8.314472 $[J/(mol \cdot K)]$
$\Delta\dot{B}$	Stream net exergy variation $[kW]$
$\Delta\eta_{ex}$	Exergy efficiency improvement index $[-]$
$\dot{B}_a$	Total available exergy $[kW]$
$\dot{B}_d$	Exergy destruction rate $[kW]$
$\dot{B}_i$	Stream exergy value of inlet flow $[kW]$
$\dot{B}_j$	Stream exergy value of outlet flow $[kW]$
$\dot{B}_u$	Total used exergy $[kW]$
$\dot{B}_{\dot{Q}}$	Heat transfer rate exergy $[kW]$
$\dot{B}_{\dot{W}}$	Mechanical power exergy $[kW]$
$\dot{B}_{d,i}$	Exergy destruction rate at the component i $[kW]$
$\dot{B}_{d,t}$	Exergy destruction rate of the system $[kW]$
$\dot{H}_{B_R}$	Power required by the boiler for reheating $[kW]$
$\dot{H}_B$	Energy provided by the boiler $[kW]$
$\dot{m}$	Stream mass flow $[kg/s]$
$\dot{m}_b$	Extracted mass flow $[kg/s]$
$\dot{m}_i$	Inlet mass flow $[kg/s]$
$\dot{m}_o$	Outlet mass flow $[kg/s]$
$\dot{m}_{11}$	Mass flow from the deareator outlet $[kg/s]$
$\dot{m}_{12}$	Mass flow through the feeding pump FP $[kg/s]$
$\dot{m}_{13}$	Mass flow at boiler inlet $[kg/s]$
$\dot{m}_{17}$	Mass flow from the turbopump $[kg/s]$
$\dot{m}_{18}$	Steam flow entering the deareator to heat the condensate $[kg/s]$
$\dot{m}_{19}$	Mass flow extracted from the high pressure turbine stage $[kg/s]$
$\dot{m}_1$	Mass flow of superheated steam from the boiler $[kg/s]$
$\dot{m}_{2.7k}$	Mass flow from the 9k line to the 2.7k line $[kg/s]$
$\dot{m}_{20}$	Mass flow extracted at the intermediate turbine pressure $[kg/s]$

$\dot{m}_{21}$	Mass flow extracted from the low pressure turbine stage $[kg/s]$
$\dot{m}_{24}$	Mass flow from the air preheater $[kg/s]$
$\dot{m}_{27}$	Mass flow from the heat exchanger drainage $[kg/s]$
$\dot{m}_{28}$	Mass flow of de-superheated steam from the boiler $[kg/s]$
$\dot{m}_{29}$	Steam mass flow used for preheating $[kg/s]$
$\dot{m}_4$	Mass flow at the low pressure turbine stage inlet $[kg/s]$
$\dot{m}_8$	Mass flow from the condenser pump $[kg/s]$
$\dot{m}_9$	Mass flow entering the heat exchanger $[kg/s]$
$\dot{m}_{aux}$	Mass flow to auxiliary heat systems $[kg/s]$
$\dot{m}_{LNG}$	Daily LNG consumption $[t/day]$
$\dot{Q}_B$	Power generated at the boiler B $[kW]$
$\dot{Q}_H$	Heat transfer rate supplied to the steam in the boiler $[kW]$
$\dot{Q}_k$	Heat transfer rate exchanged with a reservoir $[kW]$
$\dot{W}$	Mechanical power $[kW]$
$\dot{W}_t$	Turbine stage mechanical power [kW]
$\dot{W}_{CP}$	Power consumed by the drain pump CP $[kW]$
$\dot{W}_{DP}$	Power consumed by the drain pump DP $[kW]$
$\dot{W}_{MT}$	Power generated by the main turbine $[kW]$
$\dot{W}_{net}$	Net power output of the cycle $[kW]$
$\dot{W}_{TG}$	Power generated by the turbogenerator TG $[kW]$
η	Cycle efficiency $[-]$
η_B	boiler efficiency $[-]$
η_s	Isentropic efficiency $[-]$
$\eta_{ex,base}$	Exergy efficiency of the base model $[-]$
$\eta_{ex,m}$	Exergy efficiency of the modified cycle $[-]$
η_{ex}	Exergy efficiency of the total system $[-]$
$\eta_{s_{b-o}}$	Isentropic efficiency of the turbine from extraction to outlet $[-]$
$\eta_{s_{i-b}}$	Isentropic efficiency of the turbine from inlet to extraction $[-]$

ϕ_i	Influence coefficient of exergy destruction of component i [–]
AM	Amortization [€]
B_o	Boiler superheated steam outlet
B_{o_2}	Boiler de-superheated steam outlet
CCF	Cumulative Cash Flow [€]
CF	Cash Flow [€]
CPI	Consumer Price Index [%]
CV_{LNG}	LNG calorific value $[kJ/kg]$
e	Specific flow exergy $[kW/kg]$
e^{CH}	Specific chemical flow exergy $[kW/kg]$
e^{KN}	Specific kinetic flow exergy $[kW/kg]$
e^{PH}	Specific physical flow exergy $[kW/kg]$
e^{PT}	Specific potential flow exergy $[kW/kg]$
e_i	Specific flow exergy at inlet i $[kW/kg]$
e_j	Specific flow exergy at outlet j $[kW/kg]$
FS	Fuel savings [€]
h_0	Stream enthalpy at ambient reference state $[kJ/kg]$
h_b	Turbine stage extraction enthalpy $[kJ/kg]$
h_i	Inlet enthalpy, stream enthalpy $[kJ/kg]$
h_i	Turbine stage inlet enthalpy $[kJ/kg]$
h_o	Outlet enthalpy $[kJ/kg]$
h_o	Turbine stage outlet enthalpy $[kJ/kg]$
h_{10}	Enthalpy at the heat exchanger outlet $[kJ/kg]$
h_{11}	Enthalpy at the deareator outlet $[kJ/kg]$
h_{11}	Enthalpy at the feeding pump FP inlet $[kJ/kg]$
h_{12}	Enthalpy at the feeding pump FP outlet $[kJ/kg]$
h_{13}	Enthalpy at boiler inlet $[kJ/kg]$
h_{16}	Enthalpy at the turbopump TP inlet $[kJ/kg]$

h_{17}	Enthalpy at the turbopump TP outlet $[kJ/kg]$
h_{18}	Enthalpy of the steam flow entering the deareator $[kJ/kg]$
h_{19}	Enthalpy at the high pressure turbine stage extraction $[kJ/kg]$
h_1	Enthalpy of superheated steam from the boiler $[kJ/kg]$
$h_{2.7k}$	Enthalpy of the flow from the 9k line to the 2.7k line $[kJ/kg]$
h_{21}	Enthalpy at the low pressure turbine stage extraction $[kJ/kg]$
h_{24}	Enthalpy at the air preheater outlet $[kJ/kg]$
h_{27}	Enthalpy at the drain pump outlet $[kJ/kg]$
h_{28}	Enthalpy of de-superheated steam from the boiler $[kJ/kg]$
h_{29}	Enthalpy of the steam used for preheating $[kJ/kg]$
h_{30}	Enthalpy of the saturated condensate at the preheater working pressure $[kJ/kg]$
h_{33}	Enthalpy of the reheated steam $[kJ/kg]$
h_3	Enthalpy at the high pressure turbine stage outlet $[kJ/kg]$
h_8	Enthalpy at the condenser pump outlet $[kJ/kg]$
h_{9k}	Enthalpy of the 9k line $[kJ/kg]]$
h_9	Enthalpy at the heat exchanger inlet $[kJ/kg]$
h_{b_s}	Turbine stage extraction insentropic enthalpy $[kJ/kg]$
h_{o_s}	Outlet isentropic enthalpy $[kJ/kg]$
I	Investment [€]
i	Discount rate [%]
IRR	Internal Rate of Return [%]
K_{TFP}	Ratio between the work of the feeding pump FP and turbopump TP $[-]$
N	Number of components in the system $[-]$
NPV	Net Present Value [€]
NR	Net result of the year [€]
OMC	Operation and maintenance costs [€]
PBP	Pay-Back Period $[years]$

PBT	Profit Before Tax [€]
R_{CO_2}	Revenue of reduction in CO_2 emissions [€]
ROI	Return of Investment [%]
s_0	Stream entropy at ambient reference state$[kJ/(kg \cdot K]$
s_i	Stream entropy $[kJ/(kg \cdot K]$
T_0	Ambient temperature $[K]$
T_H	Temperature at the boiler $[K]$
T_k	Reservoir temperature $[K]$
TAX	Taxes [€]
x_i	Molar fraction of i-th component of the mixture
ALARP	"As Low As Reasonable Practicable" risk level area
B	Boiler
BOG	Boil-Off Gas
CP	Condensate pump
D	Deareator
DFDE	Dual Fuel Diesel Engines
DFSM	Dual Fuel Steam Turbine Mechanical
DP	Heat exchanger drain pump
FP	Boiler feeding pump
HE	Heat exchanger
HP	High pressure stage of the main turbine
LNG	Liquefied Natural Gas
LP	Low pressure stage of the main turbine
LP_b	Low pressure extraction of the main turbine
MC	Main condenser
ME-GI	Marine Engine Gas Injection
RICE	Reciprocating Internal Combustion Engines
SAH	Boiler air preheater

TG Turbogenerator

TP Turbopump

UST Ultra Steam Turbine

X-DF X Dual Fuel Engine (commercial name)

1. Introduction

In the recent years, natural gas has become relevant in the worldwide energetic landscape, mainly as a result of its role as a transitional fuel towards more renewable options [1]. The increase of its demand, altogether with the geographical distance between the main production and consumption centers, have set the focus on maritime transport, regarding logistic, economic, energetic and environmental issues. In this context, Liquefied Natural Gas (LNG) ships with suitable engine technology offer significant reductions in emissions compared to traditional marine fuels, almost eliminating NOx, SOx and particulates and reducing CO_2 emissions by up to 30% [2]. The energy-price discount, additionally, is sufficient to warrant the acquisition premium for LNG-fueled ships [3]. Regarding the safety of LNG ship operations, Vanem et al. [4] presented a risk analysis in which both individual and societal associated risk levels lie within the "As Low As Reasonable Practicable" (ALARP) area, from which safety of these operations may be implied.

With regard to logistic issues, natural gas must be cooled below -162 °C to reach liquid state (LNG) and allow greater ship load capacities [5]. Under these conditions and despite tank thermal isolation, a small fraction of the load, between 0.1 and 0.25% per day [6, 7], is naturally evaporated. This fact leads to a progressive increase in tank pressure and the need to adopt solutions to avoid overpressure. In this context, different approaches have been proposed to minimize evaporation losses in LNG transportation [8]. An option is the reliquefaction of the evaporated gas fraction, called Boil-Off Gas (BOG) [5, 9, 10]. However, this option entails additional investment and operating costs [11], so the evaporating BOG is often burnt in the ship boiler, reciprocating engines or gas turbines [7]. This also avoids direct emission of the fuel, relatively highly contaminant with respect to CO_2, to the atmosphere [5]. Due to its technical simplicity, this is the main option chosen in naval industry, employing the reaction energy as a support to ship propulsion.

An analysis of the energy efficiency of powering options for LNG ships was performed by Ekanem Attah and Bucknall [12]. Traditionally, the thermal engine that achieved energy extraction from BOG was a Rankine cycle. This cycle allows the use of combined gas or liquid fuels to support special situations, such as maneuvers, port operations or ballast navigation [5, 11], offering great versatility, reliability and security [5, 13]. Apart from the Rankine cycle, the Ultra Steam Turbine (UST) [14] or the Dual Fuel Steam Turbine Mechanical (DFSM), other technologies that allow the use of gas or liquid fuels simultaneously have emerged in the last two decades [15, 2]. These technologies, such as Dual Fuel

Diesel Engines (DFDE) [2], Marine Engine Gas Injection (ME-GI) [16] or X-DF, a commercial name for a specific Dual Fuel Engine [15], are based in Reciprocating Internal Combustion Engines (RICE) and offer a high-efficiency and a more cost-effective alternative [13, 15, 17], as shown in Table 1. Nevertheless, the new RICE-based systems still suffer from security and reliability issues and costs related to operation and maintenance [17]. This means that optimization of the Rankine cycle of LNG carriers may make steam turbine based propulsion plants competitive with these newer technologies.

Table 1: Efficiency from different LNG ship propulsion systems

System	DFSM	UST	DFDE	MEGI	X-DF
Efficiency	30%	35%	40%	50%	47%

The improvement of Rankine cycle efficiency has been under study for several decades. Superheating of steam has been already present since 1850 [18], whereas regeneration processes were firstly employed in 1876 [19]. The most common methods to improve the cycle efficiency are supercritical, reheated, regenerative and binary vapor cycles [20, 21]. Sarr and Mathieu-Potvin [19] used a refrigeration cycle to generate a low heat sink for the Rankine cycle in order to increase the Rankine cycle efficiency. Yilmazoglu [22] employed numerical simulations to investigate the effect of the heat transfer fluid and the condenser type in a Rankine cycle on the leveled cost of electricity. Su et al. [23] studied the effect of the number of regenerative stages and the feedwater temperature on the efficiency of the Rankine cycle of a nuclear power plant. Exergy analysis is a very useful tool for the assessment of the thermodynamic performance of of a Rankine cycles [24, 25]. Elsafi [26] applied an exergy analysis to the Rankine cycle of a solar power plant, with the aim of identifying the system components with the highest exergy destruction rates. Bolatturk et al. [27] did the same with a coal-powered thermal power plant. Habib and Zubair [28], by applying a second-law-based thermodynamic analysis of a regenerative-reheat Rankine cycle, found increases up to 14% in the cycle efficiency due to feedwater heating and steam reheating. Anvari et al. [29] proposed a combined heat and power plant with a regenerative organic Rankine cycle, increasing exergy efficiency in 2.6% with respect to the baseline cycle. Combinations of the Rankine cycle with other cycle types, such as Kalina, have also shown higher efficiency values [30, 31]. Another possibility to enhance the Rankine cycle efficiency is combining it with an absorption step, resulting in the so-called hygroscopic cycle [21, 32]. Finally, regarding environmental emissions, according to Beér [33], efficiency improvement is by far the most predictable and lowest cost method to reduce all emissions. Consequently, stricter emissions regulations and the variability of fuel prices [34, 35] pose the focus on the optimization of steam turbine based propulsion plants in order to continue to be considered on LNG ships [11].

Concerning the specific research on Rankine steam cycles in ships, there is not much literature available. Potential designs for new plants are being cur-

rently investigated in order to increase the efficiency of naval Rankine cycles, mainly using techniques such as steam reheating or the introduction of intermediate expansion stages [10, 14, 36]. Some simulation models for the energy system of LNG ships have been proposed by Dimopoulos and Frangopoulos [37], Mrzljak, Poljak and Mrakovčić [38] or Livanos, Theotokatos and Pagonis [39]. These models are mainly based in thermodynamic equations that represent the energy exchanges that occur inside the power plant. However, despite efficiency has been substantially improved with respect to conventional cycles, these new designs have not enjoyed great success at commercial scale [40]. In fact, since 2012, there is hardly any new order of steam-based propulsion ships [1, 13], so the market share of DFSM systems has been reduced from 72% in 2015 to 63% in 2017 and to 47% of the 525 existing ships at the end of 2018 [1].

Regarding the current DFSM fleet that is still incorporating the improvements and contributions obtained through research, the present work analyzes the energy efficiency variation of a real steam Rankine cycle installed on board a LNG transport ship. The main aim is the optimization of the propulsion plant of the ship through modifications of the thermodynamic cycle that may be performed with relative simplicity, such as the addition of reheating and preheating stages, without complex equipment. Following the cycle efficiency improvement achieved through these modifications, economic savings in fuel consumption and a revenue due to the reduction in carbon emissions may be obtained.

With this aim, a thermodynamic model of the propulsion plant, based on the facility plans and diagrams, is developed. Afterwards, the model is adjusted and validated with experimental data obtained from the actual ship operation. Finally, possible improvements of the system are tested using the model to evaluate the differences with the reference case. An exergy analysis of the impact of the cycle modifications is performed, as well as an economic analysis of the proposed investment plan. The rest of this document comprises the description of the propulsion plant, the thermodynamic model of the reference case and the studied modifications, the results of the simulations, exergy and economic analysis and the main conclusions obtained from this work.

The novelty of this work relies on the industrial application of a thermodynamic model for the optimization of the ship propulsion plant, using actual operational and experimental data from the ship utilization and showing the practical industrial application of thermodynamic and exergy analysis. In this way, an efficiency, economic and environmental improvement in a real industry is possible, beyond a theoretical analysis.

2. Description of the propulsion plant

The cycle studied is a DFSM, employed on board several twin ships for propulsion. Specifically, the thermal engine is a regenerative Rankine cycle. A general view of the actual propulsion plant addressed in this investigation is shown in Figure 1. It has the typical configuration found in the sector, with a maximum rated power of 28 MW (mechanical), which lies in the typical range of 25-30 MW found in the literature [41]. Steam generation occurs at a pressure

of 60-65 bar, reaching maximum temperatures of 520°C with a pair of steam generators [42, 43].

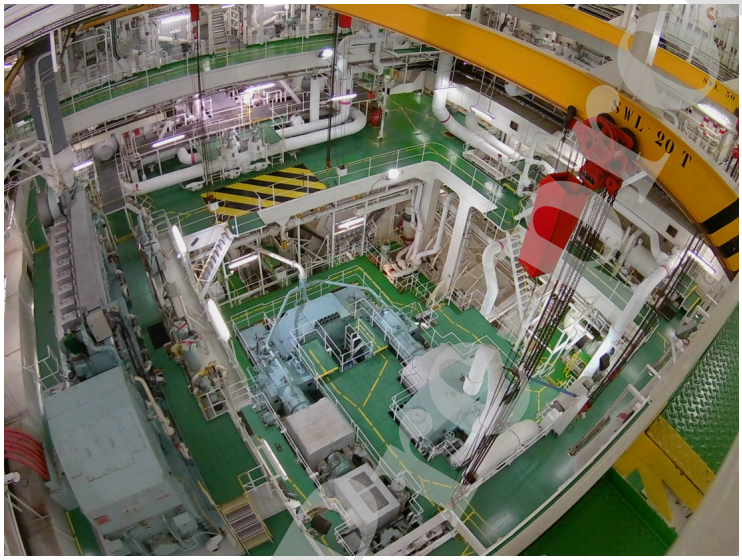

Figure 1: Propulsion plant studied in this work

The scheme of the propulsion plant used in the analysis as refence cycle to be improved is illustrated in Figure 2. The core of the propulsion plant to be modeled are the boilers, which feed a main double-stage turbine [43], electrical turbogenerators and a turbopump [38]. These boilers (B) generate steam to two main lines, one of superheated steam at 65 bar and 520°C (B_o (state 1) in Figure 2) and another one of saturated steam, B_{o_2} (state 28). The superheated vapor line feeds the ship turbines, each one with a different function. Firstly, the main turbine, responsible for ship propulsion, consists of two stages: high (HP) and low pressure (LP). Then, the turbogenerator (TG), a single-stage turbine coupled to an electrical alternator that provides electricity on board. Additionally, the superheated steam drives the turbopump (TP) that feeds the condensed steam to the boilers.

Both the main turbine and turbogenerators discharge directly to the main condenser (MC), which rejects waste heat to sea water. The turbopump, on the other hand, discharges steam to an auxiliary intermediate pressure line (2.7 kg/cm^2). The condensed steam is extracted from the main condenser using a circulating pump and is driven to a deaerator (D) passing through three preheaters. The first one is used to generate distilled water in a vacuum tank; the second one is employed to condense the steam from the shutters; and the third and biggest one preheats water by cooling the condensate obtained from the air preheater of the boiler (SAH) and condensing steam from the low pressure extraction of the main turbine (LP_b). The feeding pump (FP), driven by the turbine, pumps the condensed steam from the deaerator to the boiler.

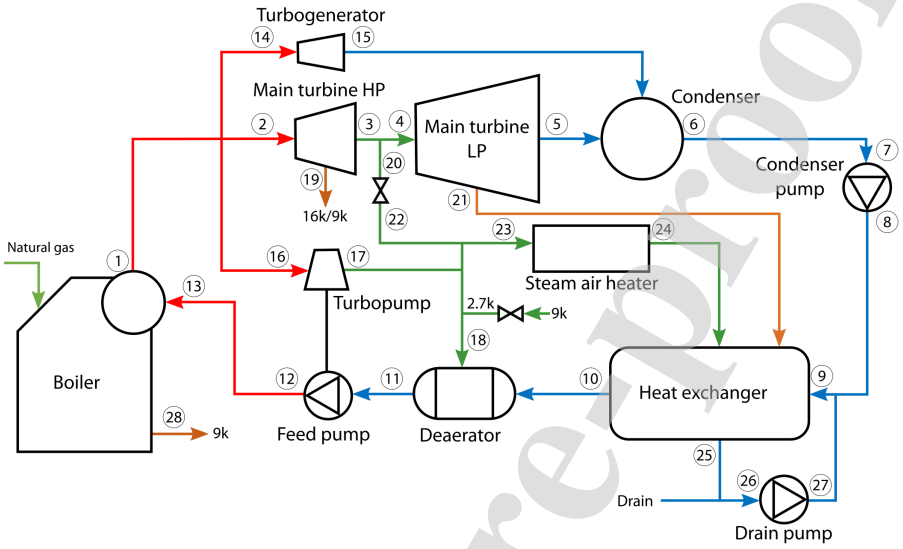

Point	Abbrev.	Description
1	B_o	Boiler superheated steam outlet
2	HP_i	High pressure stage of the main turbine inlet
3	HP_o	High pressure stage of the main turbine outlet
4	LP_i	Low pressure stage of the main turbine inlet
5	LP_o	Low pressure stage of the main turbine outlet
6	MC_o	Main condenser outlet
7	CP_i	Condensate pump inlet
8	CP_o	Condensate pump outlet
9	HE_i	Heat exchanger inlet
10	HE_o	Heat exchanger outlet
11	D_o	Deareator outlet
12	FP_o	Boiler feeding pump outlet
13	B_i	Boiler inlet
14	TG_i	Turbogenerator inlet
15	TG_o	Turbogenerator outlet
16	TP_i	Turbopump inlet
17	TP_o	Turbopump outlet
18	$D_{2.7k}$	Deareator inlet from 2.7k line
19	HP_b	High pressure turbine stage extraction
20	I_b	Intermediate turbine pressure extraction
21	LP_b	Low pressure turbine stage extraction
22	$HP_{2.7k}$	Intermediate turbine pressure extraction after depressurization to 2.7k
23	SAH_i	Boiler air preheater inlet
24	SAH_o	Boiler air preheater outlet
25	HE_b	Heat exchanger drain
26	DP_i	Heat exchanger drain pump inlet
27	DP_o	Heat exchanger drain pump outlet
28	B_{O_2}	Boiler de-superheated steam outlet

Figure 2: Scheme of the propulsion plant used to model the reference system

All these facility elements are related with each other through different auxiliary steam and condensate lines. The de-superheated steam exit feeds the 16 and 9 kg/cm^2 lines, which are related as well. The 9 kg/cm^2 line, which services auxiliary heaters, feeds also the 2.7 kg/cm^2 line. This 2.7 kg/cm^2 line services some of the most important elements of the facility, such as the deaerator.

3. Methodology

This section describes the modeling process. Firstly, the governing equations of the developed model are introduced. Then, the model is adjusted with the equipment efficiencies and coefficients obtained from the analysis of real operational data from the plant. Afterwards, the model is validated with actual values of the cycle efficiency and LNG consumption for different plant load values. Finally, the studied cycle modifications in order to improve performance are described.

3.1. Governing equations and model implementation

The thermodynamic cycle, derived from the scheme depicted in Figure 2, is the following one: an electrical pump CP extracts the condensate from the main condenser MC, which then circulates through the heat exchangers, grouped in one for the model simplicity (HE), up to the deaerator D. The condensate increases its temperature and pressure when passing through the pump. Whereas the pressure is defined by the pump specifications, the temperature rise depends on the enthalpy difference and the pump isentropic efficiency. This situation happens as well in the rest of the pumps in the facility, such as the boiler feeding pump FP and the heat exchanger drain pump DP, following the same equation:

$$h_o = h_i + \left(h_{o_s} - h_i\right)/\eta_s \tag{1}$$

where h_i and h_o are the condensate enthalpy values at the pump inlet and outlet respectively, η_s is the pump isentropic efficiency and h_{o_s} is the condensate enthalpy at the pump outlet under isentropic conditions.

Just before entering the HE, the condensate flow is mixed with another condensate coming from the auxiliary services and the drainage from the heating part of the HE itself. At this point, the enthalpy of the condensate flow increases, due to the higher temperature of the drainages, with the following equation:

$$\dot{m}_9 = \dot{m}_8 + \dot{m}_{27} \tag{2}$$

$$h_9 = \frac{\dot{m}_8 h_8 + \dot{m}_{27} h_{27}}{\dot{m}_9} \tag{3}$$

where $\dot{m}_9$ is the condensate mass flow entering the HE, $\dot{m}_8$ is the condensate mass flow from CP, $\dot{m}_{27}$ is the drainage condensate mass flow from HE and h_9, h_8 and h_{27} are the enthalpy values corresponding to these three locations.

The increase in the condensate flow enthalpy at the heat exchanger outlet is determined by the equation obtained by performing an energy balance in the HE:

$$h_{10} = h_9 + \frac{\dot{m}_{21} h_{21} + \dot{m}_{24} h_{24} - \dot{m}_{27} h_{27}}{\dot{m}_9} \tag{4}$$

where $\dot{m}_{21}$ and h_{21} are the extracted flow mass from the low pressure turbine stage LP and its enthalpy and $\dot{m}_{24}$ and h_{24} are the flow mass from the air preheater of the boiler SAH and its enthalpy.

Once the condensate reaches the deaerator, besides from becoming free from any solved gas, it is mixed with the steam used to heat and deaerate it. In these terms, the deaerator works as an open heat exchanger:

$$\dot{m}_{11} = \dot{m}_{10} + \dot{m}_{18} \tag{5}$$

$$h_{11} = \frac{\dot{m}_{10} h_{10} + \dot{m}_{18} h_{18}}{\dot{m}_{11}} \tag{6}$$

where $\dot{m}_{11}$ is the condensate flow from the deaerator outlet, $\dot{m}_{18}$ is the steam flow entering the deaerator to heat the condensate, and h_{11} and h_{18} are their respective enthalpy values.

The boiler is fed by the feeding pump FP, which is driven by a turbine TP. This is a typical configuration in this type of plants, which expand part of the main line steam in a turbine to an intermediate pressure, so that it may be pumped and used to preheat the condensate. The equation that governs the enthalpy rise in FP is the same as for the rest of the pumps, Equation 1.

Once the condensate reaches B, it is heated up to the vaporization point and then superheated up to 60-65 bar and 500-520°C. Apart from this main line exit, the boiler provides a desuperheated steam line at the same pressure and at a temperature slightly above saturation temperature. This secondary steam line is used for supporting the auxiliary lines in case the flow provided from the circuit extractions is not enough. Considering these flows, the energy that the boiler provides to the cycle may be calculated from the following expression:

$$\dot{H}_B = \dot{m}_1 h_1 + \dot{m}_{28} h_{28} - \dot{m}_{13} h_{13} \tag{7}$$

where $\dot{m}_1$ and $\dot{m}_{28}$, are the superheated and de-superheated steam flows produced in the boiler and h_1 and h_{28} their respective enthalpy values and $\dot{m}_{13}$ and h_{13} are the mass flow and enthalpy of the condensate when entering the boiler.

At the boiler exit, the generated steam feeds different systems. The superheated one feeds the main turbine stages HP and LP, the turbogenerator TG and the turbopump TP. The main turbine employs the superheated steam to propel the ship, expanding it to the pressure of the main condenser. Additionally, steam is extracted from the stages to feed the lines that preheat the condensate, so that both stages follow the same equations:

$$\dot{m}_i = \dot{m}_o + \dot{m}_b \tag{8}$$

representing the mass balance, with $\dot{m}_i$, $\dot{m}_o$ and $\dot{m}_b$ being the inlet, outlet and extracted steam flows respectively and

$$h_b = h_i - \eta_{s_{i-b}} \left(h_i - h_{b_s} \right) \tag{9}$$

$$h_o = h_b - \eta_{s_{b-o}} \left(h_b - h_{o_s} \right) \tag{10}$$

representing the enthalpy change of the steam throughout the turbine, divided into two stages separated by the steam extraction. h_i, h_o and h_b are the inlet, outlet and extracted steam enthalpy values, whereas $\eta_{s_{i-b}}$ and $\eta_{s_{b-o}}$ are the

isentropic efficiency values of the two turbine stages and h_{b_s} and h_{o_s} are the enthalpy values at the extraction and turbine outlet under isentropic conditions.

$$\dot{W}_t = \dot{m}_i h_i - \dot{m}_o h_o - \dot{m}_b h_b \tag{11}$$

is the turbine energy balance, in which $\dot{W}_t$ is the mechanical power extracted from the steam.

The same equations may be applied to TG and TP, after considering that they have no extractions.

Finally, the auxiliary steam lines that service different ship equipment and are relevant for this thermodynamic model are the following:

- 9k line: it is a 9 kg/cm^2 line that services auxiliary heating systems, fed by the desuperheated vapor from the boiler and the steam extraction from HP. lt also feeds the 2.7k line when required.

$$\dot{m}_{28} + \dot{m}_{19} = \dot{m}_{aux} + \dot{m}_{2.7k} \tag{12}$$

$$h_{9k} = \frac{\dot{m}_{28} h_{28} + \dot{m}_{19} h_{19}}{\dot{m}_{28} + \dot{m}_{19}} \tag{13}$$

  where $\dot{m}_{19}$,$\dot{m}_{aux}$ and $\dot{m}_{2.7k}$ are the mass flows the HP steam extraction and to the auxiliary heating systems and the 2.7k line. h_{9k} and h_{19} are the enthalpy values corresponding to the 9k line and the HP steam extraction.

- 2.7k line: the central ship line and the most important one regarding operational issues. It is fed from the steam extraction at the intermediate turbine pressure and at TP in order to service the deaerator and the SAH.

$$\dot{m}_{2.7k} + \dot{m}_{20} + \dot{m}_{17} = \dot{m}_{24} + \dot{m}_{18} \tag{14}$$

$$h_{2.7k} = \frac{\dot{m}_{20} h_{20} + \dot{m}_{17} h_{17} + \dot{m}_{2.7k} h_{9k}}{\dot{m}_{20} + \dot{m}_{17} + \dot{m}_{2.7k}} \tag{15}$$

  where $\dot{m}_{20}$ and $\dot{m}_{17}$ are the mass flows from the steam extraction at the intermediate turbine pressure and the turbopump. h_{20} and h_{17} are the corresponding enthalpy values. $h_{2.7k}$ is the enthalpy of the flow from the 9k line to the 2.7k line.

- 0.1k line: fed by the low pressure extraction, it only services the heat exchanger before the deaerator in this model. $\dot{m}_{21}$ and h_{21} are its mass flow and enthalpy.

The model was programmed in a self-made MATLAB code, using the free library X Steam from Holmgren [44] to retrieve the thermodynamic properties of water and steam mixtures, a full implementation of the IF-97 standard that provides very accurate steam and water properties in ranges from 0-1000 bar and 0-2000 °C. Running time of the model was less than 1 minute in a 4-nodes Intel Core i7-4790 at 3.6 GHz and 16 Gb RAM. It must be noticed that some additional assumptions have been performed, in order to maintain a certain simplicity in modeling. The 16 bar line has been suppressed, due to the insignificant flow rate under normal operational conditions. Additionally, the preheating process has been unified in a single stage.

3.2. Adjustment of the model

Once the governing equations of the model have been defined, the values of the different coefficients and efficiencies of the equipment were determined from actual operational data from the plant. 8 specific navigation situations with different load values from 30% to 100% were analyzed. Power meters were installed at the electrical equipment (turbines and pumps) to measure their power consumption, with an accuracy of ±0.15%. Several type K thermocouples (nickel-chromium) were employed to measure the inlet and outlet temperatures of the ship equipment (±0.4% accuracy). Pressure sensors with an accuracy of ±0.5% were placed to measure pressures at the equipment inlets and outlets. Finally, flowmeters were used to measure the mass flow rate in every flow stream (±0.5% accuracy). Data were collected using a SCADA from KONGSBERG [45]. The fuel consumption was monitored by the software KYMA Steam Analyzer [46]. Based on this accuracy values, the uncertainties of calculated power values and the system efficiency were estimated to be around ±0.15% and ±0.28% respectively.

ln order to adjust the turbines, the isentropic efficiency of the HP and LP stages of the main turbine, as well as the efficiencies of the feeding turbopump and the turbogenerator were obtained using Equations 9 and 10. Figure 3 collects the results from the isentropic efficiency of the turbines depending on the turbine load.

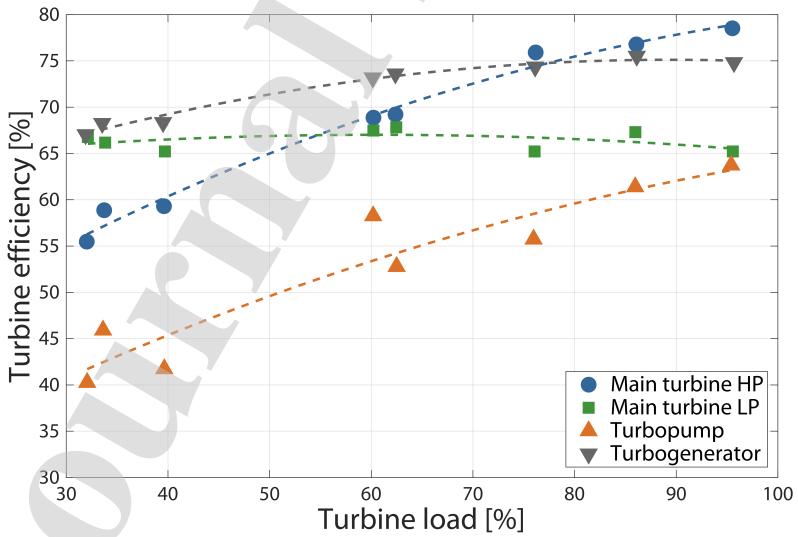

Figure 3: Insentropic efficiency of the plant turbines

The isentropic efficiency of the HP stage of the main turbine lies between 56.62 and 78.48%, with a mean value of 67.5%. For the LP stage, as no information regarding the outlet steam conditions was available, the efficiency was

calculated considering the turbine section from the stage inlet until the steam extraction, applying it to the whole turbine stage. The obtained values lie between 65.22% and 67.85%, with a mean value of 66.44%. The steam conditions at the TP outlet are also unknown, so the efficiency was obtained with the mean steam conditions at the line connected to the TP outlet. For this turbine, efficiencies from 40.35% and 63.70% were obtained, with a mean value equal to 52.57%. Finally, the TG turbine, with typically works at a load range narrower to its nominal working point, has a mean isentropic efficiency of 71.90%.

Additionally, as the turbopump TP and feeding pump FP are part of the same engine, a coefficient was calculated to relate the work obtained from the steam expanded in the turbopump and the work given to the condensate that flows to the boiler by the feeding pump:

$$K_{TFP} = \frac{\dot{m}_{12}\,(h_{12} - h_{11})}{\dot{m}_{17}\,(h_{16} - h_{17})} \tag{16}$$

where $\dot{m}_{12}$ is the mass flow through the feeding pump and h_{11} and h_{12} are the inlet and outlet enthalpy values (analogous notation for the turbopump TP). This equation allowed the calculation of the steam flow in the turbine required to pump the condensate into the boiler. From the experimental data, a mean coefficient of 0.25 was obtained for this relationship.

Regarding the isentropic efficiency of the pumps, Equation 1 was applied to the available ship data. As it may be observed in Figure 4, the pump efficiency values are more stable with load changes, showing mean values of 61.60% for FP, 92.83% for CP and 81.75% for DP.

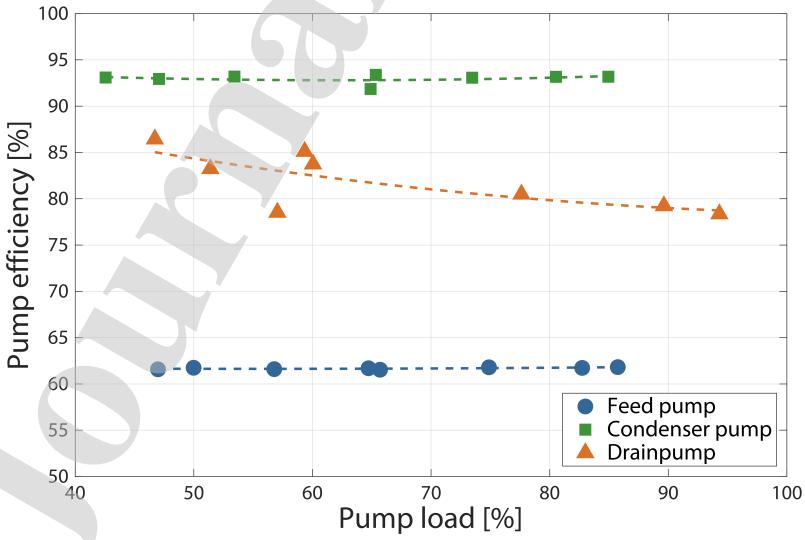

Figure 4: Insentropic efficiency of the plant pumps

Subcooling at the main condenser outlet was calculated from the difference

between the condensate temperature at the CP inlet and the saturation temperature at the MC pressure, 722 mmHg in average below atmospheric pressure. With these data, a mean subcooling of 1.0°C below saturation temperature was obtained. ln a similar fashion, condensate subcooling at the deaerator outlet was calculated from the difference of the condensate temperature at the D outlet and the saturation temperature at the D operating pressure. ln this case, the subcooling obtained was 5.2°C in average.

In order to complete the model adjustment for the boiler, the superheating of the steam at the auxiliary line from the boiler outlet has been determined. The mean difference between the temperature of the steam and the saturation temperature at the boiler working pressure is 3.5°C for the studied situations. ln order to calculate the fuel consumed by the cycle, a boiler efficiency of 87% was set, based on the technical documentation and values found in similar studies [47].

After the adjustment of the main cycle components, the losses in the steam and condensate lines were introduced. The most significant ones are produced between the boiler feeding pump (condensate) and the boiler, and at the steam feeding line to the turbines. The head loss for the first ones is the difference between the FP pressure set-point, 8100 kPa, and the boiler working pressure, depending on the plant load. On the other hand, at the steam feeding line to the turbines, a loss of 180 kPa and 5°C was found for all the analyzed cases.

Finally, the mass flow at the extractions from the main turbine has been also determined, finding that when the extraction at the high pressure is open, 2.70% of the flow rate is diverted. On the other hand, at the intermediate pressure, 5.90% of the flow is extracted. Lastly, the low pressure stage extraction diverts between 8.3 and 12.2% of the incoming flow, considering l0%, its average, as the value that was introduced in the model.

Once the model has been adjusted and all the thermodynamic variables at the different states and the energy exchanges are calculated, the cycle efficiency is obtained from the following equation:

$$\eta = \frac{\dot{W}_{MT} + \dot{W}_{TG} - |\dot{W}_{DP}| - |\dot{W}_{CP}|}{\dot{Q}_B} \tag{17}$$

where $\dot{W}_{MT}$, $\dot{W}_{TG}$, $\dot{W}_{DP}$ and $\dot{W}_{CP}$ are the values of the power produced at the main turbine and the turbogenerator, and the power consumed at the drain pump and condenser pump. $\dot{Q}_B$ is the power generated at the boiler. The sign of heat and work flow within the system boundaries have been selected according to the classical sign convention, so that heat transfer into the system and the work done by the system are considered positive; otherwise they are negative.

Additonally, the daily LNG consumption may be obtained from the calorific value of LNG and the boiler efficiency:

$$\dot{m}_{LNG} = \frac{\dot{Q}_B}{CV_{LNG}\,\eta_B} \frac{3600s}{1h} \frac{24h}{1day} \frac{1t}{1000kg} \tag{18}$$

Where CV_{LNG} is the calorific value of LNG, taken as 55731 kJ/kg, and η_B is the boiler efficiency, taken as 87%. This daily LNG consumption may be translated into daily economic expenses in fuel by multiplying it by the fuel price (14.95 €/MWh in Spain [48]).

Finally, the amount of CO_2 emitted by the direct combustion of LNG may be estimated from the chemical reaction of combustion, assuming stoichiometric combustion of methane (the main component of LNG):

$$CH_4 + 2O_2 \rightarrow CO_2 + 2H_2O \tag{19}$$

From this equation, it may be deduced that for each 16 kg of CH_4, 44 kg of CO_2 are emitted. Following this equation, it is possible to obtain the reduction of CO_2 emissions of the different modifications performed to the cycle from the difference with respect to the base model.

3.3. Model validation

The behavior of the model was compared with actual values of the cycle efficiency and LNG daily consumption for load values between 30 and 100%. As it may be observed in Figures 5 and 6, the values predicted by the model approximate reasonably well the values obtained from the actual ship functioning, especially for load values above 50%. The higher discrepancies at lower load values may be ascribed mainly to the effect of the excess steam generated with the BOG burning that flows into the condenser and the decrease in the isentropic efficiency of the turbines.

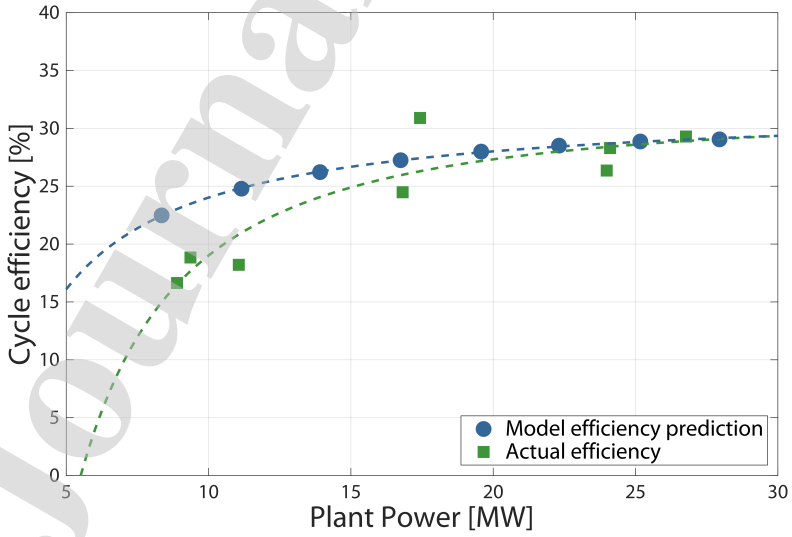

Figure 5: Validation of the model against experimental data - plant power efficiency

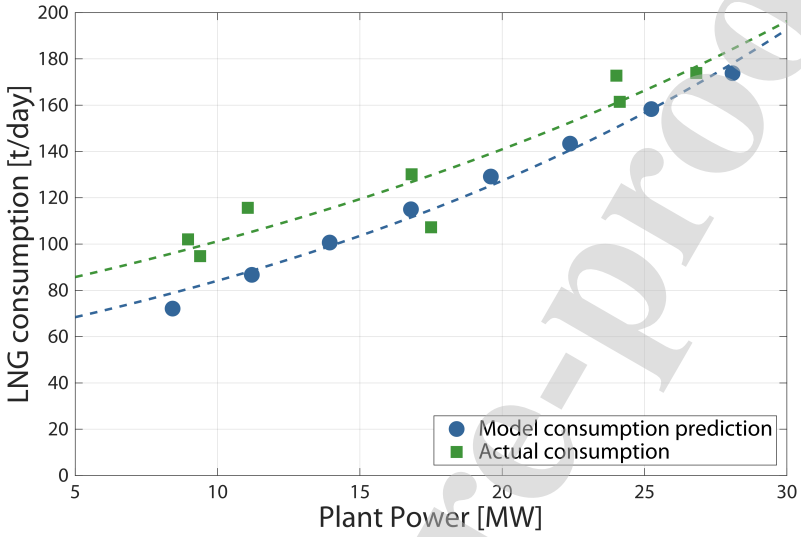

Figure 6: Validation of the model against experimental data - LNG consumption as a function of plant power

3.4. Studied modifications of the thermodynamic cycle

After validation of the model, two different modifications of the ship power plant were studied, depicted in Figure 7.

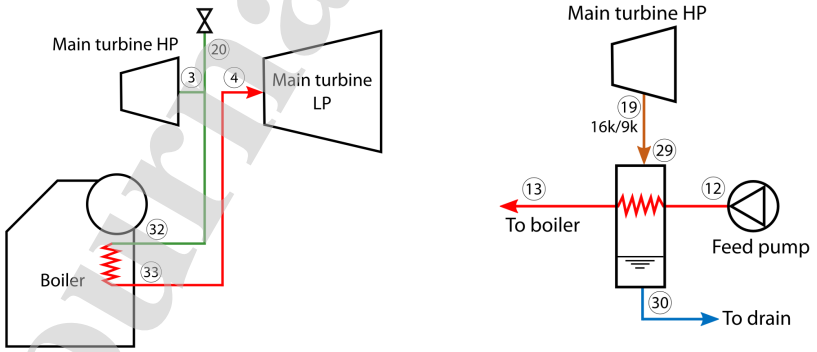

(a) Reheating

(b) Preheating

Figure 7: Modifications of the base thermodynamic cycle

- **Reheating**. A reheating stage was added just before the low pressure stage inlet of the main turbine. From the divergence after point (3) in Figure 7a, the steam flows back to the boiler and increases its temperature

up to the same value of the main line, increasing its energy subsequently and being injected back at point (4):

$$\dot{H}_{B_R} = \dot{m}_1 h_1 + \dot{m}_{28} h_{28} + \dot{m}_4 \left(h_{33} - h_{32}\right) - \dot{m}_{13} h_{13} \tag{20}$$

where $\dot{H}_{B_R}$ is the power required by the boiler, h_{33} is the enthalpy of the reheated steam and $\dot{m}_4$ is the mass flow entering the low pressure turbine stage. The thermodynamic states (32) and (33) represent the inlet and outlet of the reheater.

- **Preheating** An additional preheating stage, fed by the steam from the extraction at the high pressure stage of the main turbine (19) in Figure 7b, was placed between the boiler feeding pump and the boiler. This extracted flow from traverses the preheater, passing through states (29) and (30), corresponding to the preheater inlet and outlet, before flowing to the drain (joining state (26) depicted in Figure 2). Flow coming from the boiler feeding pump outlet (12) passes through the other side of the preheater, increasing its energy before reaching the boiler at state (13).

  Two variations were studied: in the first one, the steam is directly used from the extraction (16k). In the second one, the steam conditions are taken from one of the intermediate steam lines (9k). For both cases, the preheater follows the same equation:

$$h_{13} = h_{12} + \frac{\dot{m}_{29}\left(h_{29} - h_{30}\right)}{\dot{m}_{12}} \tag{21}$$

  Where $\dot{m}_{29}$ and h_{29} are the steam mass flow used for the preheating and its enthalpy and h_{30} is the enthalpy of the saturated condensate at the preheater working pressure.

These modifications were evaluated both individually and combined, resulting in five different situations: reheating, preheating from the 9k line, preheating from the 16k line, reheating + preheating from 9k and reheating + preheating from 16k. All the configuratíons were simulated at 80% MCR (Maximum Continuous Rate) to compare both the energy demand and efficiency of the cycle at a typical working ship load, in order to determine which configurations represent the best alternatives.

3.5. Exergoeconomic assessment

In order to complete the analysis of the different modification alternatives, an exergy analysis and an economic analysis of the possible investment plan were performed. The following subsections detail the methodology employed.

3.5.1. Exergy analysis

An exergy analysis of the different configurations was performed to obtain a better perspective of the improvements caused by the cycle modifications

[49, 50]. The exergy balance for steady flow systems was used:

$$\sum_{in} \dot{B}_i - \sum_{out} \dot{B}_j + \sum \left(1 - \frac{T_0}{T_k}\right) \dot{Q}_k - \dot{W} - \dot{B}_d = 0 \tag{22}$$

Where $\dot{B}_i$ and $\dot{B}_j$ are the exergy transfer rates at inlets and outlets respectively, $\dot{Q}_k$ is the heat transfer rate exchanged with a reservoir, T_k is the reservoir temperature, T_0 is the ambient temperature, $\dot{W}$ is the mechanical power and $\dot{B}_d$ is the exergy destruction rate.

Rates of exergy transfer at inlets and outlets are obtained as:

$$\dot{B}_i = \dot{m} e_i \qquad \dot{B}_j = \dot{m} e_j \tag{23}$$

where $\dot{m}$ is the stream mass flow and specific flow exergy e is calculated as follows [51]:

$$e = e^{PH} + e^{KN} + e^{PT} + e^{CH} \tag{24}$$

being e^{PH} the physical exergy, e^{KN} the kinetic exergy, e^{PT} the potential exergy and e^{CH} the chemical exergy. Kinetic and potential exergies e^{KN} and e^{PT} have been assumed to be negligible in this study.

The physical exergy of a stream may be obtained from the following relationship:

$$e^{PH} = (h_i - h_0) - T_0 (s_i - s_0) \tag{25}$$

where s_i is the stream entropy and h_0 and s_0 are the stream enthaply and entropy at the ambient reference state.

Additionally, the chemical exergy of a mixture may be evaluated from this equation [52]:

$$e^{CH} = \sum_i x_i \bar{e}_i^{CH} + \bar{R} T_0 \sum_i x_i log(x_i) \tag{26}$$

where x_i is the molar fraction of the i-th component of the mixture, $\bar{e}_i^{CH}$ its chemical exergy [53] and $\bar{R}$ denotes the universal gas constant.

The terms in Equation 22 may be renamed and rewritten as:

- Stream net exergy variation:

$$\Delta \dot{B} = \sum_{in} \dot{B}_i - \sum_{out} \dot{B}_j \tag{27}$$

- Heat transfer rate exergy:

$$\dot{B}_{\dot{Q}} = \sum \left(1 - \frac{T_0}{T_k}\right) \dot{Q}_k \tag{28}$$

- Mechanical power exergy:

$$\dot{B}_{\dot{W}} = \dot{W} \tag{29}$$

Consequently, Equation 22 becomes:

$$\Delta\dot{B} + \dot{B}_{\dot{Q}} - \dot{B}_{\dot{W}} - \dot{B}_d = 0 \tag{30}$$

And the exergy efficiency of the total system becomes:

$$\eta_{ex} = \frac{\dot{B}_u}{\dot{B}_a} \tag{31}$$

Where $\dot{B}_u$ and $\dot{B}_a$ are the used exergy and available exergy respectively. Additionally, in the case of a Rankine power plant, the exergy efficiency may be also defined as:

$$\eta_{ex} = \frac{\dot{W}_{net}}{\left(1 - \frac{T_0}{T_H}\right)\dot{Q}_H} \tag{32}$$

Where $\dot{W}_{net}$ is the net power output of the cycle, $\dot{Q}_H$ is the heat transfer rate supplied to the steam in the boiler and T_H is the temperature at the boiler.

In order to determine the influence of every system component in the total exergy performance of the system, its influence coefficient of exergy destruction may be calculated. The influence coefficient of exergy destruction of the component i, ϕ_i, is defined as the ratio of the exergy destruction rate at the component, $\dot{B}_{d,i}$, to the total exergy destruction rate of the system, $\dot{B}_{d,t}$:

$$\phi_i = \frac{\dot{B}_{d,i}}{\dot{B}_{d,t}} \tag{33}$$

If N is the total number of components of the system, the following equations apply:

$$\dot{B}_{d,t} = \sum_{i=1}^{N} \dot{B}_{d,i} \tag{34}$$

$$\sum_{i=1}^{N} \phi_i = 1 \tag{35}$$

In this sense, ϕ_i represents the weight of the component i in the total performance decrease of the system. Therefore, it may be used to identify the component with the greatest negative impact on the system efficiency. Finally, once the exergy efficiency of the system has been assessed, the improvement produced by the modifications performed may be quantified with the exergy efficiency improvement index, $\Delta\eta_{ex,m}$:

$$\Delta\eta_{ex,m} = \frac{\eta_{ex,m} - \eta_{ex,base}}{\eta_{ex,base}} \tag{36}$$

Where $\eta_{ex,m}$ and $\eta_{ex,base}$ are the exergy efficiencies of the modified cycle and base model respectively.

For the calculations performed in this work, ambient temperature and pressure were taken from atmospheric conditions (25 °C and 1 bar), whereas the temperature at the boiler was taken as the adiabatic flame temperature of 2100 °C, according to the data presented in [54]. Sea water temperature was assumed to be 7 °C.

3.5.2. Economic analysis

Apart from the exergy assessment, once a suitable modification from the studied ones was found, an economic analysis was performed to provide deeper insight into the viability of the related plant modification investment project.

The investment project has been calculated for 20 years, assuming that the amortization period of the new equipment is 10 years. Starting with an initial investment (I_0), four different scenarios have been studied as a function of the ship capacity utilization (i.e., the percentage of time of the year in which the ship is navigating) with the values 60, 70, 80 (provided from the ship owner) and 90%. All the calculations have been made from the difference in the economic values with respect to the base model. Investments (I), amortizations (AM), fuel savings (FS), operation and maintenance costs (OMC) are considered to calculate the Profit Before Tax (PBT), assuming a 1% per year increase in the Consumer Price Index (CPI). Then, taxes (35%, TAX) are applied to the total PBT. The revenue of the reduction in CO_2 emissions is also considered (R_{CO_2}), taking a value of 14.50 €/t, below the average values in Europe [55], in order to present a more conservative scenario for the project. Then, from the net result of the year (NR), the Cash Flow (CF) is obtained. This procedure is made explicit in the following equations:

- Profit Before Tax

$$PBT = -I + FS - AM - OMC \tag{37}$$

- Taxes

$$TAX = 0.35\, PBT \tag{38}$$

- Net result of the year

$$NR = PBT - TAX + R_{CO_2} \tag{39}$$

- Cash Flow

$$CF = NR + AM \tag{40}$$

Once the Cash Flow for every year has been obtained, the Cumulative Cash Flow (CCF) is calculated for every year y as:

$$CCF = \sum_{j=0}^{y} CF(j) \tag{41}$$

Where $CF(j)$ represents the cash flow in the year j.

Finally, the following metrics to evaluate the investment plan are calculated solving the corresponding equations:

- Net Present Value (NPV)

$$\sum_{j=0}^{20} \frac{CF(j)}{(1+i)^j} \tag{42}$$

Where the discount rate i has been taken as 5%.

- Pay-Back Period (PBP)

$$\sum_{j=0}^{PBP} CF(j) = 0 \tag{43}$$

- Internal Rate of Return (IRR)

$$\sum_{j=0}^{20} \frac{CF(j)}{(1+IRR)^j} \tag{44}$$

- Return of Investment (ROI)

$$ROI = \frac{CCF(20) - I_0}{I_0} \tag{45}$$

4. Results and discussion

4.1. Cycle efficiency, economic and environmental implications

The results obtained show that the cycle efficiency, defined by Equation 17, improves with respect to the baseline model (Figure 8). For a 80% MCR situation, the model shows a cycle efficiency of 28.94%, which translates into 144.13 t/day of natural gas consumption. The efficiency value is in line with the results presented by Fernández et al. [11].

The introduction of a reheating stage before the low pressure stage of the turbine improves slightly this efficiency, up to 29.57%, thus reducing LNG daily consumption down to 141.10 t. However, this modification results in two main differences with respect to the baseline cycle. Firstly, the steam comes out of the main turbine in superheated conditions. Secondly, the mass balance in the auxiliary lines causes the maximum possible extraction values at the high and medium pressure stages of the turbine to decrease down to 2.1% and 5.2% respectively, due to the consumption reduction in the auxiliary systems. As a consequence, the load balance in both turbine stages becomes shifted, with the low pressure stage generating more power than the high pressure one.

On the other hand, preheating the inlet flow to the boiler with steam from the first turbine extraction at the extraction conditions results in a decrease of the cycle efficiency down to 28.87% and an increase of the fuel daily consumption of 0.44 t, thus, becoming the modíficación that offers the worst results. Nevertheless, if the preheating stage is performed with steam from the 9 kg/cm^2

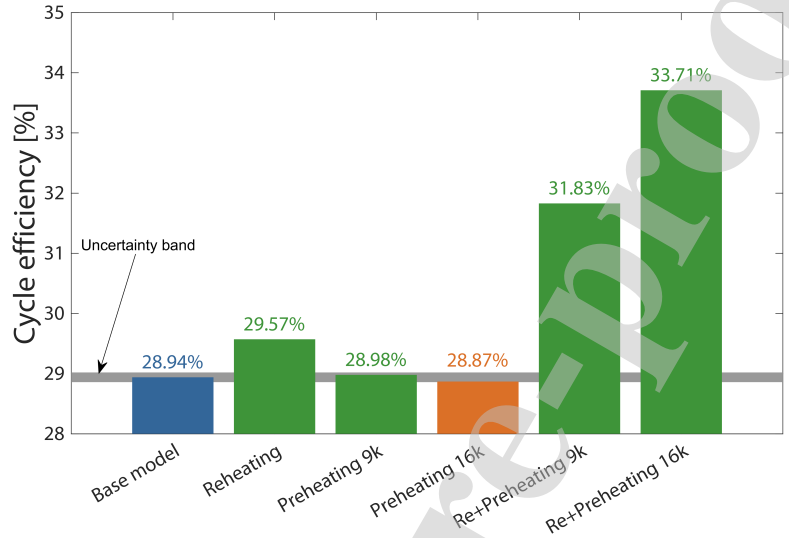

Figure 8: Plant power efficiency values with the modifications studied

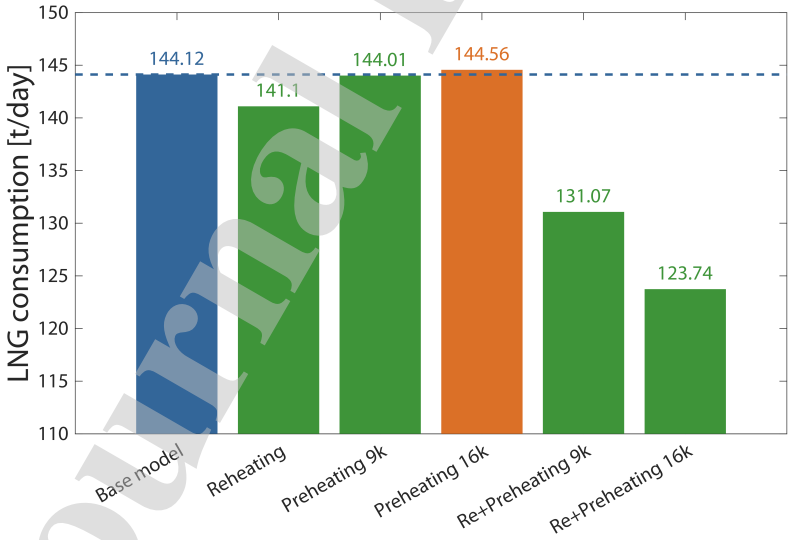

Figure 9: LNG daily consumption values with the modifications studied

auxiliary line, the cycle efficiency improves slightly up to 28.98%, reducing daily fuel consumption in 0.11 t. The difference between these two situations lies in the required amount of steam extracted from the high pressure stage of the turbine. Although the high pressure steam allows to increase the feeding water

pressure to a higher temperature, the condensation process produces less heat (1922.6 kJ/kg at 1700 kPa vs 2012.9 kJ/kg at 1010 kPa). Thus, the amount of steam to be extracted in the high pressure stage of the turbine becomes higher, resulting in a higher steam amount to be produced in the boiler for the same turbine power. A comment about these two cases must be made, as their efficiency lies within the uncertainty limits of the base model case. Therefore, the results corresponding to these two preheating cases should be taken with caution. On the other hand, they are not the most interesting ones, as they do not represent a major improvement of the system efficiency.

The best results have been obtained for the situations that combine both reheating and preheating. In this case, reheating while preheating with steam from the 16 kg/cm^2 line, contrary to the previous situation, increases substantially the cycle efficiency with respect to the baseline case, up to 33.71%, an increase of performance comparable to the Ultra Steam Turbine [14, 11]. Using steam from the 9 kg/cm^2 line, on the other hand, represents an increase in efficiency up to 31.83%. Fuel consumption reduction becomes relevant with these two modifications, being 20.38 and 13.05 t/day respectively.

Economic implications of these improvements determine their viability for possible remodeling projects. Therefore, only the modifications that achieve higher efficiency improvements are to be considered, i.e., the ones combining reheating and preheating. Consequently, with a market price of 14.95 €/MWh in Spain [48], savings up to 4681.94 €/day could be generated for 80% MCR load values by preheating the boiler feeding water with a steam extraction at the high pressure stage of the turbine and reheating the steam that enters the low pressure stage of the turbine.

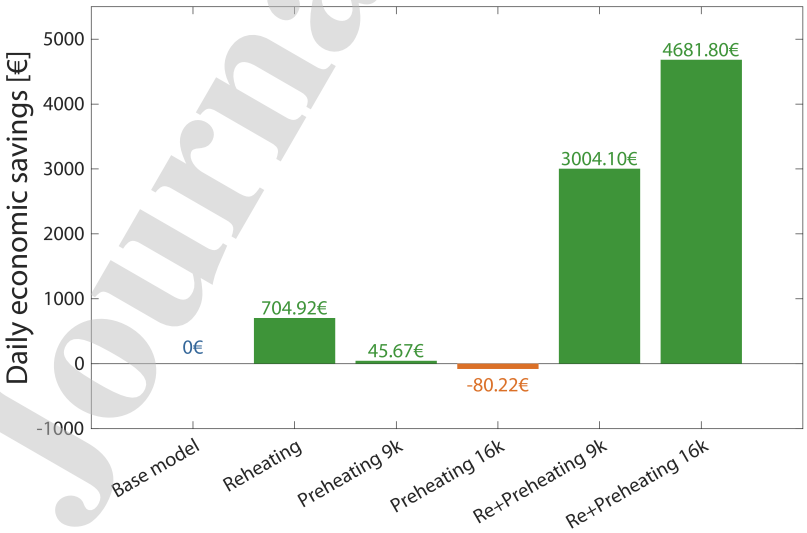

Figure 10: Daily economic savings with the modifications studied

Additionally, significant cuts with respect to yearly CO_2 emissions ascribed to LNG combustion may be observed for the cycle modifications combining reheating and preheating. Particulary, for the cycle that combines reheating and preheating with steam from the 16k line, more than 20,000 t/yr of CO_2 stop being emitted. The result is a reduction of slightly above 14% in CO_2 direct emissions, beneficial regarding both environmental issues and economic environmental costs (ecological taxation), apart from the obvious prevention of BOG emissions.

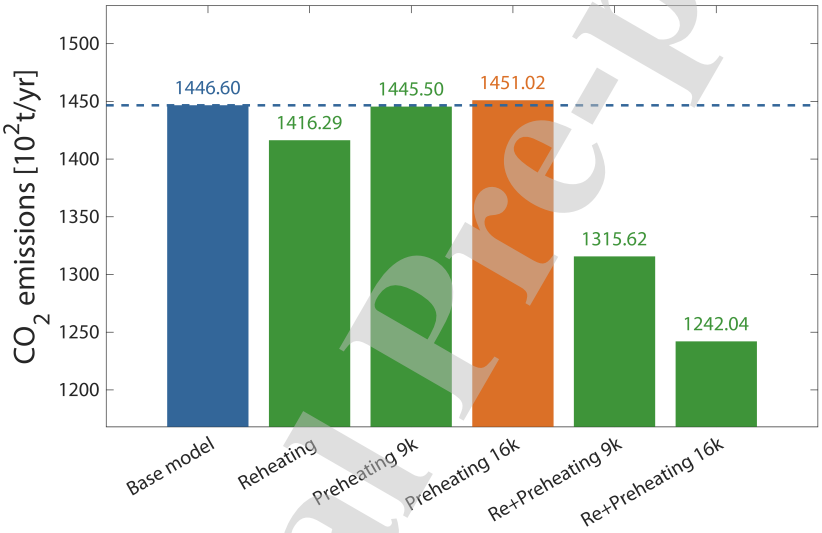

Figure 11: Daily CO_2 emissions with the modifications studied

4.2. Modifications of the thermodynamic cycle

Regarding thermodynamic aspects of the power plant cycles, Figures 12 to 17 show the thermodynamic cycles of the base model (original configuration) and all the studied configurations.

Figure 12 shows the thermodynamic cycle of the original configuration. The path from the boiler up to the high pressure stage of the turbine is marked in red. The water follows an isobaric heating process, reaching a the maximum temperature of 509.6 °C. Afterwards, the steam is diverted to the high pressure stage of the turbine (orange), to the turbopump (green) and to the turbogenerator (blue). There are three returning lines, one (green) corresponding to the mixture at the air preheater and two (blue) corresponding to the steam extraction at the low pressure stage of the turbine and the final turbine expansion respectively. The outlet of the condenser, the different pumps and the heat exchanger all fall on the saturated liquid curve.

Reheating the steam after expansion in the high pressure stage of the turbine results in an increase of the work obtained by the turbine, but, at the same

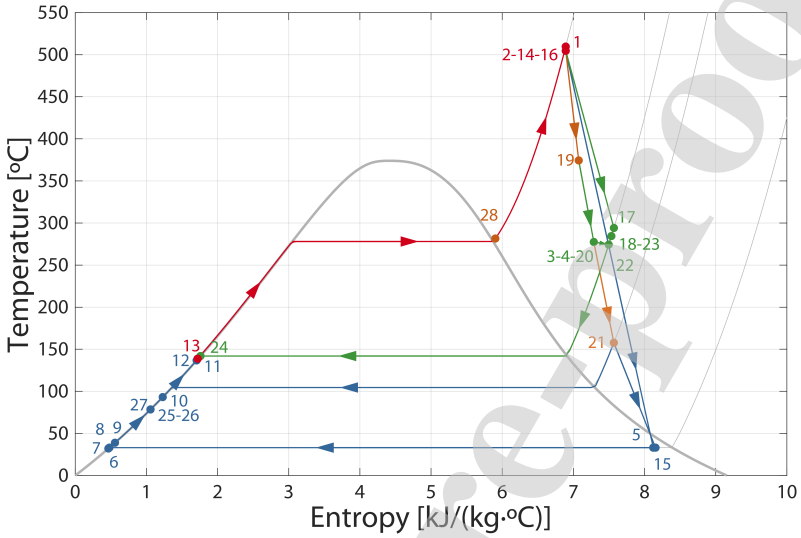

Figure 12: T-s diagram of the base model at 80% MCR

time, the turbine outlet is displaced onto the superheated vapor zone, as shown in Figure 13. Although the steam could be further expanded and this might be seen as an inefficiency, the truth is that more power is obtained, the cycle is more efficient and less fuel is required to feed the power plant. Additionally, there is no risk of liquid phase appearing in the turbine low stage.

With the addition of a preheating stage, a new returning line appears in the graph of the thermodynamic cycle, painted in orange in Figures 14 and 15. This complication of the cycle and the addition of the preheating equipment are a priori unjustified, as the cycle efficiency does not increase substantially and it even decreases when the preheating is performed using the 16k line.

Nevertheless, combinations of both preheating and reheating show promising results. Figures 16 and 17 show the thermodynamic cycles of the configurations with reheating and preheating from the 9k and 16k lines respectively. The power generated at the turbine increases substantially while the necessary fuel amount to generate that power is reduced significantly. As observed with the plain reheating situation, the output of the low pressure stage of the turbine is also displaced out to the superheated vapor region, increasing thus the useful life of the turbine. As previously mentioned, this does not translate in a loss of power generation; on the contrary, the turbine power output increases significantly.

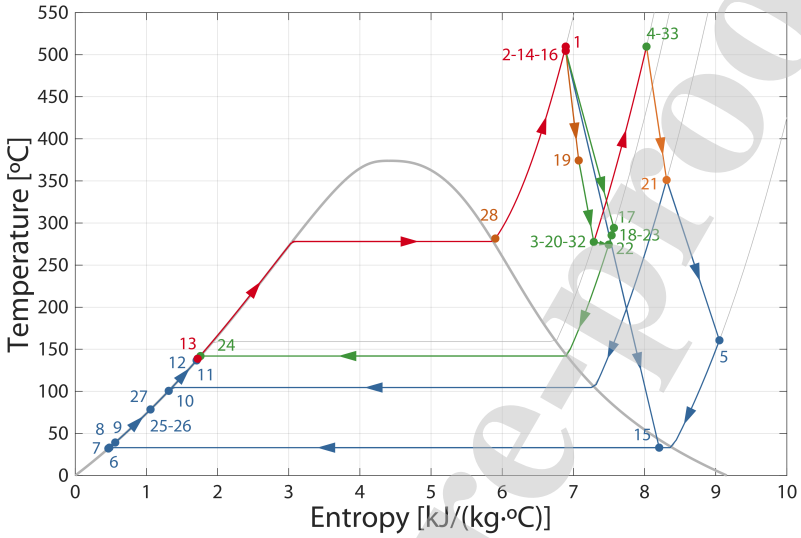

Figure 13: T-s diagram of the model with reheating at 80% MCR

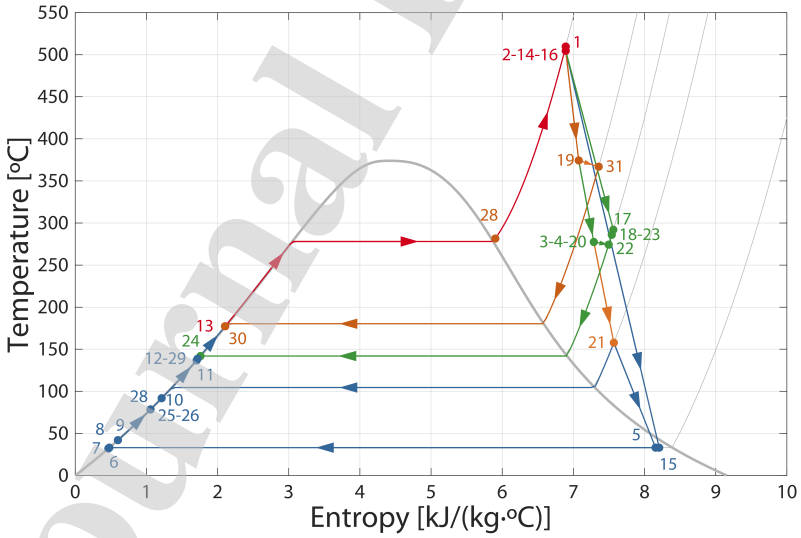

Figure 14: T-s diagram of the model with preheating from the 9k line at 80% MCR

4.3. Exergy analysis

The results of the exergy analysis of the base model are collected in Table 2:

It may be appreciated that the highest contributor to exergy destruction is the boiler, with more than 60% of exergy destruction ocurring at this compo-

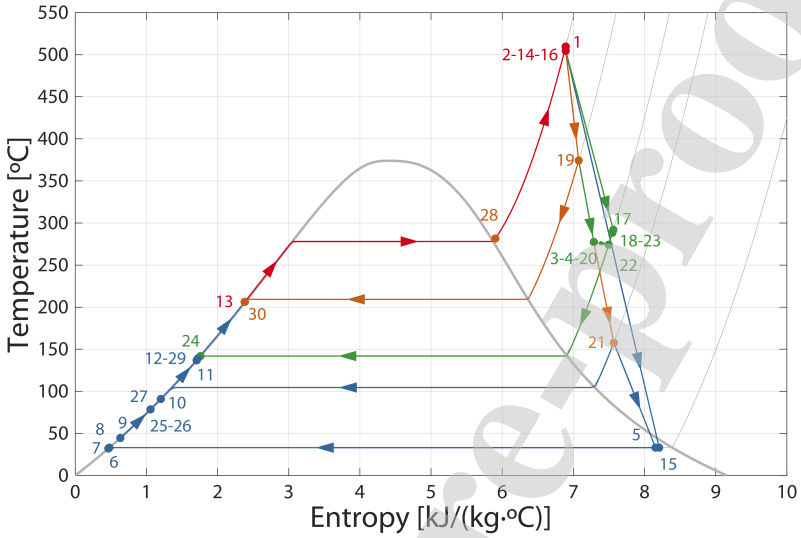

Figure 15: T-s diagram of the model with preheating from the 16k line at 80% MCR

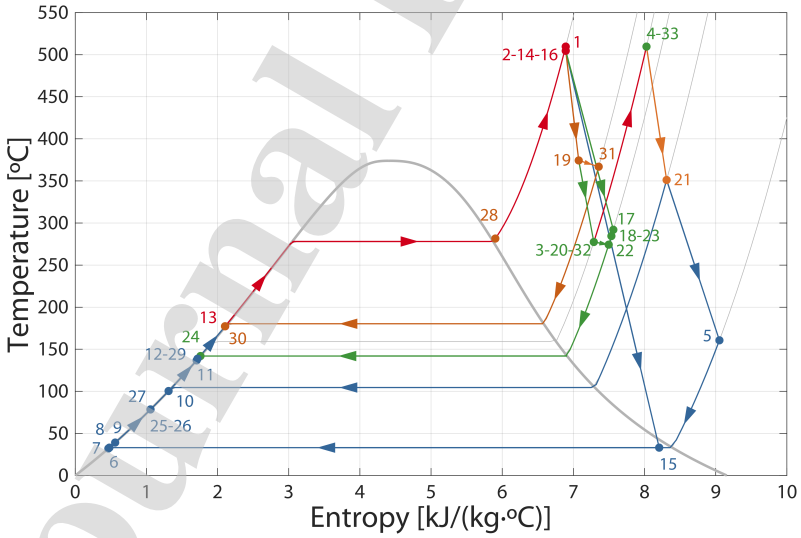

Figure 16: T-s diagram of the model with preheating from the 9k line and reheating at 80% MCR

nent.The exergy supplied in the boiler to the stream is around 72.3 MW, but the exergy destruction rate is almost 51.7 MW. Therefore, modifications trying to increase energy utilization at the boiler seem the most suitable ones to increase

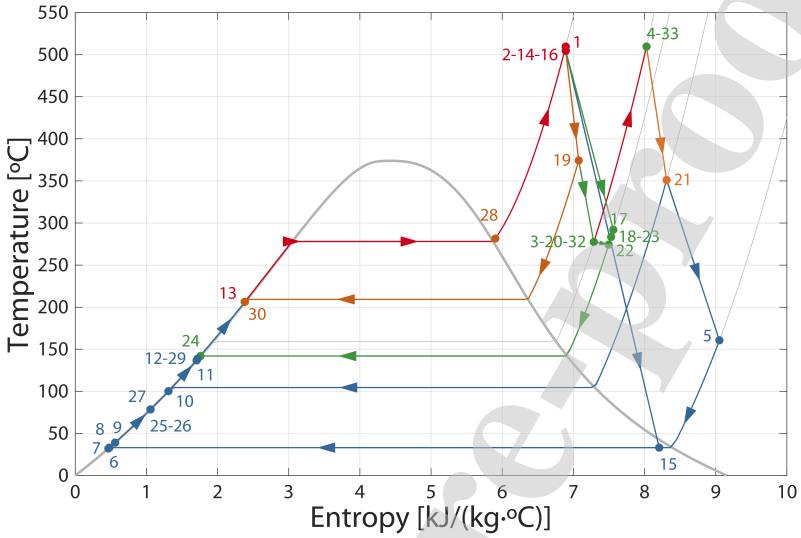

Figure 17: T-s diagram of the model with preheating from the 16k line and reheating at 80% MCR

Table 2: Exergy analysis of the base model

Element	$\Delta\dot{B}\,[kW]$	$\dot{B}_{\dot{Q}}\,[kW]$	$\dot{B}_{\dot{W}}\,[kW]$	$\dot{B}_d\,[kW]$	$\phi_i\,[\%]$
Boiler	31642.76	0.00	0.00	31642.76	61.22
HP turbine	13645.87	0.00	10659.46	2986.40	5.78
LP turbine	17448.68	0.00	11740.54	5708.15	11.04
Heat exchanger	564.46	0.00	0.00	564.46	1.09
Deaerator	310.61	0.00	0.00	310.61	0.60
Turbopump	908.33	0.00	591.20	317.13	0.61
Feed pump	-213.56	0.00	-591.20	377.65	0.73
Turbogenerator	2154.85	0.00	1561.17	593.68	1.15
Steam Air Heater	731.13	-192.36	0.00	538.77	1.04
Condenser	1453.27	3464.26	0.00	4917.53	9.51
Other elements*	3725.97	0.00	0.00	3725.97	7.21
Other pumps	-7.94	0.00	-8.75	0.81	0.00
Total				**51683.93**	100.00

*intermediate pressure lines, valves and pipes

the overall cycle efficiency. Modifications such as re- or preheating the steam, in line with the modifications studied in this work. The condenser and the low pressure stage of the turbine account for around 10% of the exergy destruction each, in line with the results from [26], who claimed that particular attention should be paid to the heat source, condenser, low pressure turbine and high pressure turbine (in that particular order) because they constitute the major

sources of exergy destruction."

The exergy efficiency of the studied modifications and the respective improvements are collected in Table 3. It may be observed that only the modifications that combine reheating and preheating offer a significant improvement over the base cycle. From the results of the efficiency analysis, the most suitable option is the modification with preheating from the 16k line and reheating, being able to improve the system exergy efficiency more than 16%.

Table 3: Exergy efficiency of the studied cycle modifications

Cycle	Base model	Reheating	Preheating 9k	Preheating 16k	Reheating + Preheating 9k	Reheating + Preheating 16k
Exergy efficiency [%]	33.09	33.82	33.14	33.02	36.40	38.55
Exergy efficiency improvement [%]	-	2.19	0.14	-0.25	9.98	16.51

The detailed results of the exergy analysis of this option are shown in Table 4:

Table 4: Exergy analysis of the model with preheating from 16k line and reheating

Element	$\Delta\dot{B}\,[kW]$	$\dot{B}_{\dot{Q}}\,[kW]$	$\dot{B}_{\dot{W}}\,[kW]$	$\dot{B}_d\,[kW]$	$\phi_i\,[\%]$
Boiler & Reheater	21528.60	0.00	0.00	21528.60	52.16
HP turbine	12082.62	0.00	9470.47	2612.15	6.33
LP turbine	18455.20	0.00	12929.53	5525.67	13.39
Heat Exchanger	648.70	0.00	0.00	648.70	1.57
Deaerator	194.08	0.00	0.00	194.08	0.47
Turbopump	755.23	0.00	491.55	263.67	0.64
Feed pump	-177.56	0.00	-491.55	313.99	0.76
Turbogenerator	2212.19	0.00	1561.17	651.03	1.58
Steam Air Heater	627.79	-165.16	0.00	462.63	1.12
Preheater	491.30	0.00	0.00	491.30	1.19
Condenser	2048.77	3261.06	0.00	5309.83	12.87
Other elements*	3270.93	0.00	0.00	3270.93	7.93
Other pumps	-6.67	0.00	-7.35	0.68	0.00
Total				**41273.26**	100.00

*intermediate pressure lines, valves and pipes

Exergy destruction has been reduced from almost 51.7 MW to slightly above 41.2 MW for the same plant power output (less than 80% of the original value), thanks to the reheating and preheating from the 16k line processes. As a consequence, the contribution of the boiler to exergy destruction has been reduced to 52.16 % from the original 61.22%, a reduction of more than 14%. This proves that reheating and preheating have a very positive effect on the boiler performance. As a consequence, the influence coefficients of the condenser and the

turbine stages rise with respect to the base model. Nevertheless, the modifications performed have a strong positive effect in the global efficiency.

4.4. Economic analysis of the selected modification

From the previous analyses, the modification option with reheating and preheating with steam from the 16k line is the one that increases the cycle efficiency in a higher degree, resulting in higher economic savings and reduction of CO_2 emissions. The initial investment for implementing these modifications in the current Rankine cycle is $I_0 = 7{,}614{,}858.33$ €, according to the information provided by the company. The amortization costs, thus, become $AM = 76{,}1485.83$ €/year during the first 10 years of the investment. The fuel savings in the first year $FS(1)$ with the cycle modifications have a value of 1,367,085.60 €, whereas the operation and maintenance costs, according to the information provided by the company, entail $OMC(1) =$ 228,445.75 €. With these data, the Profit Before Tax for the first year becomes $PBT(1) =$ 377,154.02 €, so that the first year taxes are $TAX(1) =$ 132,003.91 €. With the revenue of the reduction in CO_2 emissions being $R_{CO_2} =$ 296,612 €, the net result of the first year becomes $NR(1) =$ 541,762.11 € and the cash flow $CF(1) =$ 1,303,247.94 €. Table 5 collects the results of the investment for the most representative years (rounded to €) to show the evolution of the cash flow.

Table 5: Investment plan showing the most representative years

Year	0	1	2	...	6	7	...	19	20
I [€]	7,614,858	0	0	...	0	0	...	0	0
FS [€]	0	1,367,086	1,380,756	...	1,436,821	1,451,189	...	1,635,236	1,651,588
OMC [€]	0	228,446	230,730	...	240,099	242,500	...	273,255	275,987
AM [€]	0	761,486	761,486	...	761,486	761,486	...	0	0
BAT [€]	-7,614,858	377,154	388,540	...	435,236	447,203	...	1,361,981	1,375,601
TAX [€]	0	132,004	135,989	...	152,333	156,521	...	476,693	481,460
R_{CO_2} [€]	0	296,612	296,612	...	296,612	296,612	...	296,612	296,612
NR [€]	-7,614,858	541,762	549,163	...	579,515	587,294	...	1,181,900	1,190,753
CF [€]	-7,614,858	1,303,248	1,310,649	...	1,341,001	1,348,780	...	1,181,900	1,190,753
CCF [€]	-7,614,858	-6,373,670	-5,184,872	...	-910,241	48,312	...	7,684,642	8,133,424

This investment plan has a Net Present Value $NPV = 8,133,424.29$ €, and the Pay-Back Period PBP extends up to 6 years and 347 days. The Internal Rate of Return is $IRR = 16.14$ % and the return of investment is 6.81%. These metrics indicate that the investment plan is profitable and, thus, the advice for the company would be to engage in the modification of the cycle.

With the aim of testing the sensitivity of these results with respect to the ship utilization capacity, Figures 18 and 19 show the influence of this factor on the CCF (Figure 18) and on the PBP and the IRR (Figure 19). It may be appreciated that the four scenarios show promising investment perspectives, as IRR is always above 12% and the PBP is always below 9 years.

5. Conclusions

Stricter emission regulations and the variability of fuel prices set the focus on the optimization of steam turbine based propulsion plants in order to

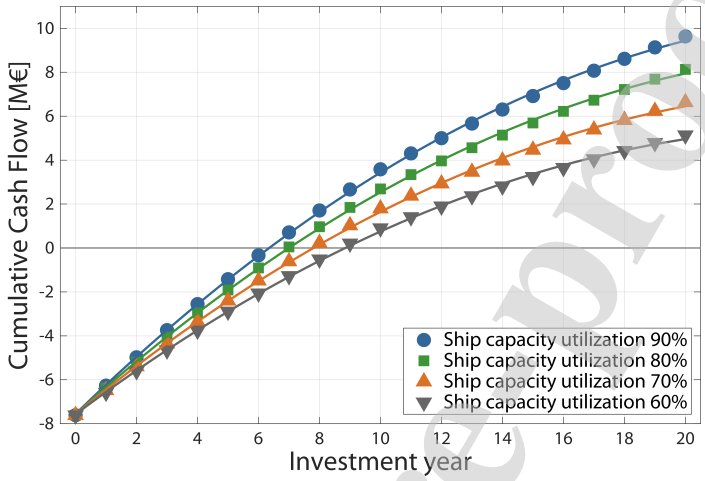

Figure 18: Cumulative Cash Flow as a function of the ship capacity utilization

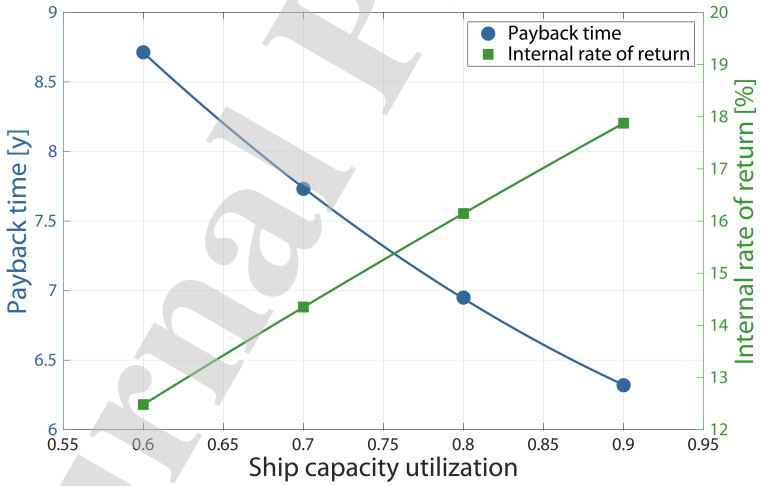

Figure 19: Pay-Back Period and Internal Rate of Return as a function of ship capacity utilization

continue to be considered for Liquefied Natural Gas (LNG) transport ships. Current research lines are focused on the introduction of reheating, preheating or intermediate expansion stages. The efficiency of a propulsion plant for a LNG transport ship has been improved in this work by studying possible modifications of the regenerative Rankine cycle used for propulsion that would not entail complex investments or modifications, like the addition of reheating and preheating stages.

A thermodynamic model of the propulsion plant has been developed from the facility plans and diagrams, able to predict the ship behavior with reasonable accuracy, regarding the available experimental data. The values obtained for the cycle efficiency are consistent with the data available in the literature. Additionally, the predictions of different scenarios obtained by the model when introducing modifications in the power propulsion cycle showed promising results. Particularly, it was found that combinations of steam reheating and preheating stages are able to optimize the cycle efficiency, achieving the same amount of power generation at the expense of a lower fuel consumption. A combination of preheating with the 16 kg/cm^2 line available in the ship and reheating after the expansion at the high pressure turbine stage is the most promising alternative, increasing the cycle efficiency from 28.94% to 33.71%.

Hence, economic savings in fuel consumption and a revenue due to the reduction in carbon emissions may be obtained. The selected option reduces the fuel consumption in 20.38 t/day, resulting in savings up to almost 4700 €/day when the ship moves at 80% load charge. Additionally, the reduction in CO_2 emissions ascribed to fuel combustion as a result of this modification reaches up to more than 20,000 tn per year. All these results are supported by the modifications performed in the thermodynamic cycles, which also highlight the total elimination of liquid phase in the turbine low pressure stage.

An exergy analysis of the impact of the cycle modifications was performed, as well as an economic analysis of the proposed investment plan. It was found that the boiler was the main contributor to exergy destruction, result in line with results from other authors. This fact justifies that the modifications performed in the cycle should be directed towards improving the boiler exergy efficiency (reheating and preheating). The economic analysis of the investment plan of implementing the selected alternative showed promising results even in a conservative scenario, with very beneficial investment metrics, with an Internal Rate of Return higher than 12% and a Pay-Back Period less than 9 years for all the studied scenarios.

In summary, a suitable alternative for enhancing the performance of the propulsion plant of a LNG ship has been proposed in this work, increasing its efficiency, reducing fuel consumption and greenhouse emissions and potentially saving money. A practical industrial application of thermodynamic and exergy analysis beyond theory has been shown, allowing an efficiency, economic and environmental improvement in a real industry. Future works should focus on analyzing further modifications of the cycle to increase the exergy efficiency of other equipment, as well as studying different ship working load regimes for longer cruising times.

References

[1] International Gas Union. 2019 World LNG Report. Technical report, Barcelona, Spain, 2019.

[2] V. Æsoy, P.M. Einang, D. Stenersen, E. Hennie, and I. Valberg. LNG-Fuelled Engines and Fuel Systems for Medium-Speed Engines in Maritime Applications. Technical Report 2011-01-1998, SAE International, Warrendale, PA, USA, Aug 2011.

[3] O. Schinas and M. Butler. Feasibility and commercial considerations of LNG-fueled ships. *Ocean Engineering*, 122:84–961, 2016.

[4] E. Vanema, P. Ant ao, I. Østvik, and D. Del Castillo de Comas. Analysing the risk of LNG carrier operations. *Reliability Engineering and System Safety*, 93:1328–1344, 2008.

[5] G. McGuire and B. White. *Liquefied Gas Handling Principles on Ships and in Terminals*. Witherby, Livingston, UK, 2000.

[6] D. Dobrota, B. Lalić, and I. Komar. Problem of Boil-off in LNG Supply Chain. *Transactions on Maritime Science*, 2:91–100, 2013.

[7] P. Głomski and R. Michalski. Problems with determination of evaporation rate and properties of boil-off gas on board LNG carriers. *Journal of Polish CIMA*, 6:133–140, 2011.

[8] M.M.F Hasan, A.M. Zheng, and I.A. Karimi. Minimizing Boil-Off Losses in Liquefied Natural Gas Transportation. *Industrial & Engineering Chemistry Research*, 48:9571–9580, 2009.

[9] T.N. Anderson, M.E. Ehrhardt, R.E. Foglesong, T. Bolton, D. Jones, and A. Richardson. Shipboard Reliquefaction for Large LNG Carriers. In H.E. Alfadala, G.V. Rex Reklaitis, and M.M. El-Halwagi, editors, *Proceedings of the 1st Annual Gas Processing Symposium*, volume 1, pages 317–324, Amsterdam, NL, 2009. Elsevier.

[10] J. Romero Gómez, M. Romero Gómez, R. Ferreiro Garcia, and A. De Miguel Catoira. On board LNG reliquefaction technology: a comparative study. *Polish Maritime Research*, 21:77–88, 2014.

[11] I.A. Fernández, M.R. Gómez, J.R. Gómez, and Á.B. Insua. Review of propulsion systems on LNG carriers. *Renewable and Sustainable Energy Reviews*, 67:1395–1411, 2017.

[12] E. Ekanem Attah and R. Bucknall. An analysis of the energy efficiency of LNG ships powering options using the EEDI. *Ocean Engineering*, 110:62–74, 2015.

[13] K. Kosowski. Steam turbine as the main ship propulsion. More than a hundred years at sea. In *21st Scientific Session on Marine Technology*, Gdańsk, Poland, 2004. Gdańsk University of Technology.

[14] M. Ito, K. Hiraoka, S. Matsumoto, and K. Tsumura. Development of high efficiency marine propulsion plant (Ultra Steam Turbine). Technical Report Vol. 44 No. 3, Mitsubishi Heavy Industries, Ltd., Tokyo, Japan, Sep 2007.

[15] H. Tu, F. Hongjung, L. Wei, and Z. Guoqiang. Options and Evaluations on Propulsion Systems of LNG Carriers. In A. Serpi and M. Porru, editors, *Propulsion systems*, chapter 1, pages 1–20. IntechOpen, London, UK, 2019.

[16] P. Skjoldager. Propulsion of LNG Carriers by MAN B&W Two-Stroke Diesel Engines. *Marine Engineering*, 40:328–333, 2005.

[17] D. Chang, T. Rhee, K. Nam, K. Chang, D. Lee, and S. Jeong. A study on availability and safety of new propulsion systems for LNG carriers. *Reliability Engineering & System Safety*, 93:1877–1885, 2008.

[18] J.H. White. *A History of the American Locomotive: Its Development, 1830-1880*. Dover Publications, Mineola, NY, USA, 1979.

[19] J.A.R. Sarr and F. Mathieu-Potvin. Increasing thermal efficiency of rankine cycles by using refrigeration cycles: a theoretical analysis. *Energy Conversion and Management*, 121:358–379, 2016.

[20] Y.A. Çengel and M. Boles. *Thermodynamics: An Engineering Approach 8th Ed.* McGraw-Hill Education, New York, NY, USA, 2014.

[21] F.J. Rubio-Serrano, A.J. Gutiérrez-Trashorras, F. Soto-Pérez, E. Álvarez Álvarez, and E. Blanco-Marigorta. Advantages of incorporating Hygroscopic Cycle Technology to a 12.5-MW biomass power plant. *Applied Thermal Engineering*, 131:320–327, 2018.

[22] M.Z. Yilmazoglu. Effects of the selection of heat transfer fluid and condenser type on the performance of a solar thermal power plant with technoeconomic approach. *Energy Conversion and Management*, 111:271–278, 2016.

[23] Y. Su, K.S. Chaudri, W. Tian, G. Su, and S. Qiu. Optimization study for thermal efficiency of supercritical water reactor nuclear power plant. *Energy Conversion and Management*, 63:541–547, 2014.

[24] W. Wang, S. Deng, D. Zhao, L. Zhao, S. Lin, and M. Chen. Application of machine learning into organic Rankine cycle for prediction and optimization of thermal and exergy efficiency. *Energy Conversion and Management*, 210:112700–1–22, 2020.

[25] W. Sun, X. Yue, and Y. Wang. Exergy efficiency analysis of ORC (Organic Rankine Cycle) and ORC-based combined cycles driven by low-temperature waste heat. *Energy Conversion and Management*, 135:63–73, 2017.

[26] A.M. Elsafi. Exergy and exergoeconomic analysis of sustainable direct steam generation solar power plants. *Energy Conversion and Management*, 103:338–347, 2015.

[27] A. Bolatturk, A. Coskun, and C. Geredelioglu. Thermodynamic and exergoeconomic analysis of Çayirhan thermal power plant. *Energy Conversion and Management*, 101:371–378, 2015.

[28] M.A. Habib and S.M. Zubair. Second-law-based thermodynamic analysis of regenerative-reheat Rankine-cycle power plants. *Energy*, 17:295–301, 1992.

[29] S. Anvari, S.Jafarmadar, and S. Khalilarya. Proposal of a combined heat and power plant hybridized with regeneration organic Rankine cycle: Energy-Exergy evaluation. *Energy Conversion and Management*, 122:357–365, 2016.

[30] X. Zhang, M. He, and Y. Zhang. A review of research on the Kalina cycle. *Renewable and Sustainable Energy Reviews*, 16:5309–5318, 2012.

[31] R.S. Murugan and P.M.V. Subbarao. Thermodynamic analysis of Rankine-Kalina combined cycle. *International Journal of Thermodynamics*, 11:133–141, 2008.

[32] F.J. Rubio-Serrano, F. Soto-Pérez, and A.J. Gutiérrez-Trashorras. Experimental study on the influence of the saline concentration in the electrical performance of a Hygroscopic cycle. *Applied Thermal Engineering*, 165:114588–1–10, 2020.

[33] J.M. Beér. High efficiency electric power generation: the environmental role. *Progress in Energy and Combustion Science*, 33:107–134, 2007.

[34] D. Maxwell and Z. Zhu. Natural gas prices, LNG transport costs, and the dynamics of LNG imports. *Energy Economics*, 33:217–226, 2011.

[35] D. Maxwell and Z. Zhu. Improving sustainability of maritime transport through utilization of liquefied natural gas (LNG) for propulsion. *Energy*, 57:412–420, 2013.

[36] E. Querol, B. Gonzalez-Regueral, J. García-Torrent, and A. Ramos. Available power generation cycles to be coupled with the liquid natural gas (LNG) vaporization process in a Spanish LNG terminal. *Applied Energy*, 88:2382–2390, 2011.

[37] G.G. Dimopoulos and C.A. Frangopoulos. Thermoeconomic Simulation of Marine Energy Systems for a Liquefied Natural Gas Carrier. *International Journal of Thermodynamics*, 11:195–201, 2008.

[38] V. Mrzljak, I. Poljak, and T. Mrakovčić. Energy and exergy analysis of the turbo-generators and steam turbine for the main feed water pump drive on LNG carrier. *Energy Conversion and Management*, 140:307–323, 2017.

[39] G.A. Livanos, G. Theotokatos, and D.-N. Pagonis. Techno-economic investigation of alternative propulsion plants for Ferries and RoRo ships. *Energy Conversion and Management*, 79:640–651, 2014.

[40] S. Grzesiak. Alternative Propulsion Plants for Modern LNG Carriers. *New Trends in Production Engineering*, 1:399–407, 2018.

[41] W.J. Fox and S.C. MacBirnie. *Marine Steam Engines and Turbines*. Newnes-Butterworths, Oxford, UK, 1970.

[42] R.P. Sinha and W.M.N.W. Nik. Investigation of propulsion system for large LNG ships. *Materials Science and Engineering Conference Series*, 36:012004, Sep 2004.

[43] C. Behrendt and A. Adamkiewicz. LNG carrier power systems. *Rynek Energii*, 88:55–62, 2010.

[44] M. Holmgren. X Steam, Thermodynamic properties of water and steam. MATLAB Central File Exchange. `https://www.mathworks.com/matlabcentral/fileexchange/9817-x-steam-thermodynamic-properties-of-water-and-steam`, 2020. Accessed: 2020-07-28.

[45] KONGSBERG. K-CHIEF Automation System. `https://www.kongsberg.com/maritime/products/engines-engine-room-and-automation-systems/automation-safety-and-control/vessel-automation-k-chief/`, 2020. Accessed: 2020-07-28.

[46] KYMA. KYMA Steam Analyzer. `https://kyma.no/kyma-steam-analyzer/`, 2020. Accessed: 2020-17-28.

[47] V. Mrzljak, I. Poljak, and V. Medica-Viola. Dual fuel consumption and efficiency of marine steam generators for the propulsion of LNG carrier. *Applied Thermal Engineering*, 119:331–346, 2017.

[48] MIBGAS - Mercado Ibérico del Gas. `http://www.mibgas.es/mercados-de-gas/`. Accessed: 2019-06-12.

[49] T.J. Kotas. *The exergy method of thermalplant analysis*. Butterworth, London, UK, 1985.

[50] M.J. Moran and E. Sciubba. Exergy Analysis:Principles and Practice. *Journal of Engineering for Gas Turbines and Power*, 116:285–290, 1994.

[51] M. Olfati, M. Bahiraei, and F. Veysi. A novel modification on preheating process of natural gas in pressure reduction stations to improve energy consumption, exergy destruction and CO2 emission: Preheating based on real demand. *Energy*, 173:598–609, 2019.

[52] M. Olfati, M. Bahiraei, S. Heidari, and F. Veysi. A comprehensive analysis of energy and exergy characteristics for a natural gas city gate station considering seasonal variations. *Energy*, 155:721–733, 2018.

[53] S.C. Kaushik and O.K. Singh. Estimation of chemical exergy of solid, liquid and gaseous fuels used in thermal power plants. *Journal of Thermal Analysis and Calorimetry*, 115:903–908, 2014.

[54] R. Lugo, M. Salazar, J.M. Zamora, A. Torres, and M. Toledo. Análisis exergético de una central termoeléctrica. *Científica*, 13:17–25, 2009.

[55] P. Criqui, M. Jaccard, and T. Sterner. Carbon taxation: A tale of three countries. *Sustainability*, 11:6280–1–21, 2019.

CRediT author statement

Andrés Meana-Fernández: Methodology, Software , Formal analysis, Validation , Data Curation , Visualization, Writing - Original Draft; **Bernardo Peris-Pérez:** Conceptualization, Methodology, Software, Formal analysis, Writing - Review & Editing; **Antonio José Gutiérrez-Trashorras:** Conceptualization, Methodology, Formal analysis, Writing - Review & Editing, Supervision, Project administration; **Santiago Rodríguez-Artime:** Conceptualization, Methodology, Software, Validation, Formal analysis, Investigation, Resources; **Juan Carlos Ríos-Fernández:** Data Curation, Writing - Original Draft; **Juan Manuel González-Caballín:** Data Curation, Writing - Review & Editing

***Declaration of Interest Statement**

Declaration of interests

☒ The authors declare that they have no known competing financial interests or personal relationships that could have appeared to influence the work reported in this paper.

☐The authors declare the following financial interests/personal relationships which may be considered as potential competing interests:

HIGHLIGHTS

- Development of a thermodynamic model of the ship propulsion plant
- Experimental validation with actual operation data from the ship
- Preheating and reheating effects on the cycle efficiency are assessed
- Cycle efficiency is improved, fuel consumption and CO2 emissions are reduced
- Exergy and economic assessment of the cycle improvement